Consequences of thermal aging on the detection of impact damage in composite structures with PZT/FBG guided wave systems

Loïc Mastromatteo, Ludovic Gavérina, Jean-Michel Roche, Florian Lavelle, François-Xavier Irisarri

eJNDT e-Journal of Nondestructive Testing - ISSN 1435-4934 - www.ndt.net

EWSHM 2024
11th European Workshop on Structural Health Monitoring

Consequences of thermal aging on the detection of impact damage in composite structures with PZT/FBG guided wave systems

Loïc MASTROMATTEO [1,2], Ludovic GAVERINA [1], Jean-Michel ROCHE [1], Florian LAVELLE [2], François-Xavier IRISARRI [1]
[1] ONERA, Paris-Saclay University, F-92322 Châtillon, FRANCE
loic.mastromatteo@onera.fr
[2] CNES, 75012 Paris, FRANCE

Abstract. This paper studies the detection of barely visible impact damage in composite plates with guided waves (GW) based SHM systems and focuses on how this detection is affected by the degradation of the sensors potentially induced by the exposition to thermal cycling. Two frequencies are investigated to test both fundamental Lamb waves modes (A0 at 25 kHz and S0 at 200 kHz). Two different types of sensors are tested (commonly used piezoelectric PZT transducers and Fiber Bragg Grating (FBG) sensors) which provide very similar results in term of GW measurements. Sensors degradation is monitored through diagnostic measurements based on Electromechanical Impedance (EMI) measurements and Laser Doppler Vibrometry (LDV) scans for PZT and measurements of the reflection spectrums for the FBG. As degradation of an SHM system can also comes with evolutions of the bonding layers, two different bonding methods were tested: bonding with a secondary adhesive and cobonding on composite surface during the curing process.

The effects of the damage and the sensors degradation due to the thermal cycling are compared through their influence on a commonly used damage index (DI) based on cross-correlation with the baseline signals. Cobonded sensors showed a very good stability to the thermal cycling exposition for both the “diagnostic” measurements and the GW signals, which allows a good detection of the impact damage above 7.5J of impact energy. On the contrary, for bonded sensors, significant degradations were detected mainly with the appearance of debondings under some of the PZT discs which lead to DI values up to the values corresponding to a 10J impact damage that would therefore lead to false detection. However, those degradations were easily identifiable with the diagnostic measurements of the corresponding sensors, therefore those GW acquisitions could be flagged as faulty to avoid a false detection. These results will likely strongly depend on the choice of the DI and therefore other common DI formulations should be tested and presented at the conference.

Keywords: Guided Waves (GW), Impact damage detection, Sensor durability, Piezoelectric Wafer Active Sensor (PWAS), Fiber Bragg Grating (FBG)

https://doi.org/10.58286/29816

Introduction

In the context of recent reusable launch vehicles (RLV) developments, SHM could help fast and economic revalidation of RLVs between launches, provided that the transducers keep their functionality and reliability after repeating launches being exposed to harsh flight conditions. This paper studies the detection of barely visible impact damage in composite plates with guided waves (GW) based SHM systems. More precisely, it focuses on how this detection can be affected by the degradation of the sensors potentially induced by the exposition to flight conditions. The aging conditions in this work mainly consist of thermal cycling with high maximum temperature (150°C), expected for RLV structures and close to the operational limit of the thermoset-matrix composites. The response of the sensors to such environmental conditions depends on the sensors themselves and on their bonding to the structure. Thus, in this paper two different types of sensors are compared (commonly used PZT transducers and Fiber Bragg Grating (FBG) sensors) along with two different bonding methods (classic bonding with a secondary adhesive and cobonding on composite surface during the curing process). Sensor diagnostic measurements are used to assess the sensor degradation after the thermal cycling. These diagnostic measurements are based on Laser Doppler Vibrometry [1], [2] and Electromechanical Impedance measurements (EMI) [3] for the PZT and a monitoring of the reflection spectrum for the FBG.

Two identical instrumented composite plates are manufactured for this work. The first to serve as reference for the impact damage detection and the second to assess the influence of the thermal cycling on the GW signals and sensors degradations. Sensors are setup in pairs (PZT-PZT or PZT-FBG) with GW signal paths going through the impact location. After a baseline acquisition on both plates, incremental impact tests (with increasing energy) are performed up to 12.5 J on the first plate while the second plate is submitted to thermal cycling. The influence of the damage and the sensors degradation due to the thermal cycling are then compared through their effect on the common Signal Difference Coefficient (SDC) damage index (DI) to identify if the sensors degradation might lead to false detection (mistaking sensor degradation for structural damage) when using this particular DI. For the sake of brevity, a single DI is tested in this paper. However many other DI formulations exist in the literature (a few of them can be found in [4] for example) that could lead to various results with different sensitivity to both the impact damage and sensor degradations. The tests of other common DI formulations are under progress and will be presented at the conference.

The present paper is divided in the following sections: the experimental setup is first introduced (Section 2), then results of the diagnostic step after thermal cycling are presented (Section 3) followed by the impact damage detection (Section 4) and conclusions (Section 5).

2. Experimental setup

2.1 Materials and sensor Layout

Two identical T700/M21 GC quasi-isotropic CFRP composite plates ([0,45,90,-45]s layout) with dimensions of 400 mm x 400 mm were manufactured for this study. On each plate are attached two networks of four sensors as showed in Fig. 1. The third system visible on the plate is part of another study. The incremental impact is located in the middle of the plate and of the two sensors networks. Both networks are composed of one PZT-PZT pair and one PZT-FBG pair. PZT are C-6 PZT discs from Fuji-Ceramics and FBG are uniform FBG available in the commerce. Each network is attached using a different bonding process.

One network is cobonded onto the plate in autoclave: the sensors (PZT and FBG) are directly placed on the uncured composite laminate before the curing of the host composite plate. The second network is bonded on the plate using a consumer grade cyanoacrylate adhesive (LOCTITE 495). A one-kilogram weight is used to apply a constant pressure onto the PZT discs during the adhesive cure, resulting in an adhesive thickness of about 30 µm. According to the manufacturer's datasheet, the adhesive strength is expected to drop significantly at the highest temperatures of the considered thermal cycle (-50% at 120°C). Such adhesive choice was made on purpose, in order to increase the chances of witnessing the consequences of significant evolutions of the adhesive layer.

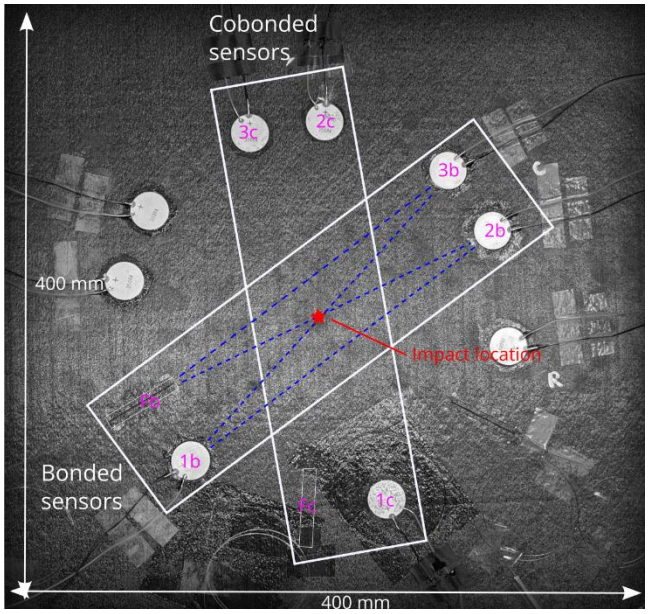

Fig. 1. Composite plate layout, investigated wave paths are denoted in blue dotted lines and PZT are labelled as they will be referred to in the rest of the article.

2.2 Thermal cycling setup

The second composite plate is submitted to five thermal cycles in a climatic chamber up to a maximum temperature of 150°C to match the maximum temperature that a composite RLV structure might be subjected to under its thermal protection. Each cycle is relatively short (about 15 minutes) similarly to the short duration flight expected for an RLV first stage. Previous works soon-to-be-published by the authors showed that such thermal cycles should lead to degradation of the bonding layer with potential debondings along with an alteration of the piezoelectric properties of the PZT discs. The FBG sensors however are expected to not be deteriorated as much as the PZT sensors.

2.3 Lamb wave pitch catch measurements

The lamb wave signals are investigated along the different paths going through the impact location that are drawn on Fig. 1. PZT excitation voltage is a 10 Vpp, 3-cycle hanning windowed sinusoidal toneburst. Two frequencies are tested corresponding to the maximum amplitudes of emission of both the fundamental lamb wave modes according to the lamb wave tuning principle [5, pp. 309–362]. The anti-symmetric mode (A0) is measured at 25 kHz and the symmetric mode (S0) at 200 kHz. GW measurements with FBGs are done using an accordable laser tuned to the slope of their reflection spectrums. A description of this

interrogation technique can be found in [6] along with other techniques for ultrasonic measurements with fiber optic sensors. Fig. 2 shows an example of the recorded signals for two equivalent paths between two PZT (path 21) and between a PZT and an FBG (path 3F) before any impact.

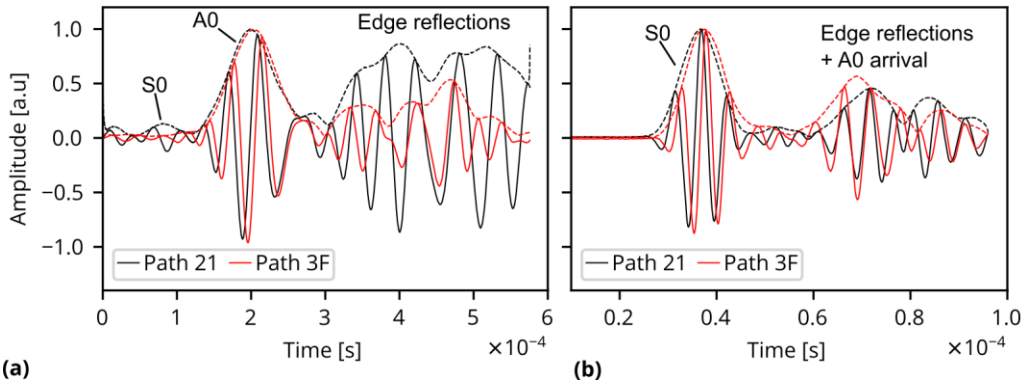

Fig. 2. Recorded Lamb wave signals and their envelope for plate 1 in a pristine state at 25 kHz (a) and 200 kHz (b). Signals are plotted for two equivalent paths between two PZT (path 21) and a PZT and an FBG (path 3F).

For both frequencies, the signals recorded from the FBG and from the PZT are very similar for the direct wave packet with only some slight delay that may be explained by small uncertainties in the sensors positioning. However, the difference is sharper for the edge reflections as they come to the sensors from various angles and the FBG GW sensitivity is directional and therefore depends on the incident signal direction. In order to avoid the influence of the edge reflections due to the relatively small size of the composite plate, signals are windowed to study only the direct wave signals.

2.4 Damage index

In order to compare the baseline signals to the signals on impacted or thermally aged plate, a common damage index (DI), called Signal Difference Coefficient (SDC) [4] is assessed. This DI directly derives from the cross-correlation coefficient ρ between the signal and the baseline with the following expression $SDC = 1 - \rho$. In the presence of damage, the correlation between the signal and the baseline will decrease leading to an increasing value of the DI. A similar DI was used along with a modified RAPID algorithm to detect and localize impact damage at different impact energies in glass-fiber composites [7].
The DI is presently calculated for all the GW paths at the different impact energies for the first plate and after the thermal cycling for the second plate.

3. Thermal aging: diagnostic measurements of the SHM sensors

3.1 PZT diagnostic through LDV and admittance spectrums

LDV is a Non-Destructive Technique used to measure the normal speed of a surface; it is often used to monitor guided waves propagation in structures as illustrated in [8] in comparison with a FE modelling approach of low velocity impact damage. In this work, it is mainly used to detect the presence of PZT transducer local debondings by imaging the velocity field at the surface of the transducer itself, as debonded areas are expected to have higher amplitudes of local vibration than the rest of the transducer that is restrained by the coupling with the structure as illustrated in [1], [2]. In previous works by the authors [2], PZT

vibration frequency was 25 kHz however the minimum size of the visible debondings with this method depends on the frequency at which the PZT is vibrating. Therefore, in this work, PZT are imaged with LDV at 250 kHz to detect smaller debondings. Fig. 3 shows the Root Mean Squared images of the velocity measured by LDV for PZT #1b and PZT #1c in emission at 250 kHz, before and after the thermal cycling.

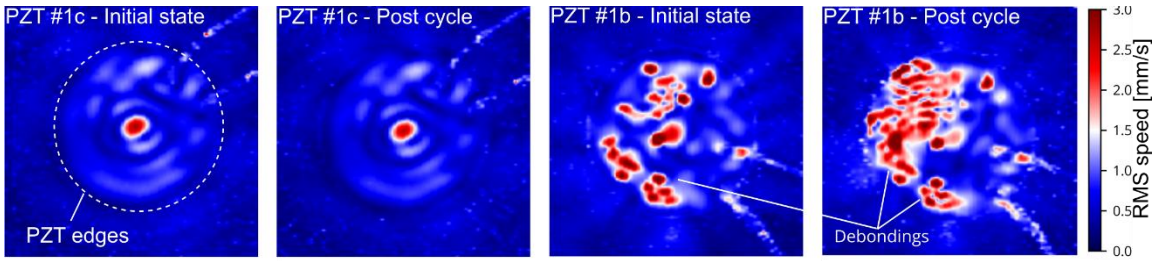

Fig. 3. RMS speed images obtained by LDV for cobonded PZT#1c and bonded PZT#1b in emission at 250 kHz before and after the thermal cycling.

We can see that the LDV scans at 250 kHz enable the detection of small debondings which would be invisible at 25 kHz. These small debonding are likely caused by small air bubbles trapped in the adhesive layer during the bonding process and those bubbles were detected for all secondary bonded transducers but not on the cobonded ones. In order to get rid of these bubbles it might be necessary to add a vacuum bagging step in the bonding. Even if these small debondings do not significantly affect the GW generation or sensing by the transducer, they might create some initiation points to propagate into bigger debondings during thermal cycling for example. Indeed, we can see that after the thermal cycling PZT#1b presents a larger debonded area, which is also the case for PZT#3b while none of the cobonded sensors exhibited such debondings.

Since LDV inspection might not be possible in the case of a real RLV structure protected by a thermal protection, measurements of the admittance spectrum of the PZT sensors are also performed to monitor the degradation of the sensors under the thermal cycling as presented in Fig. 4.

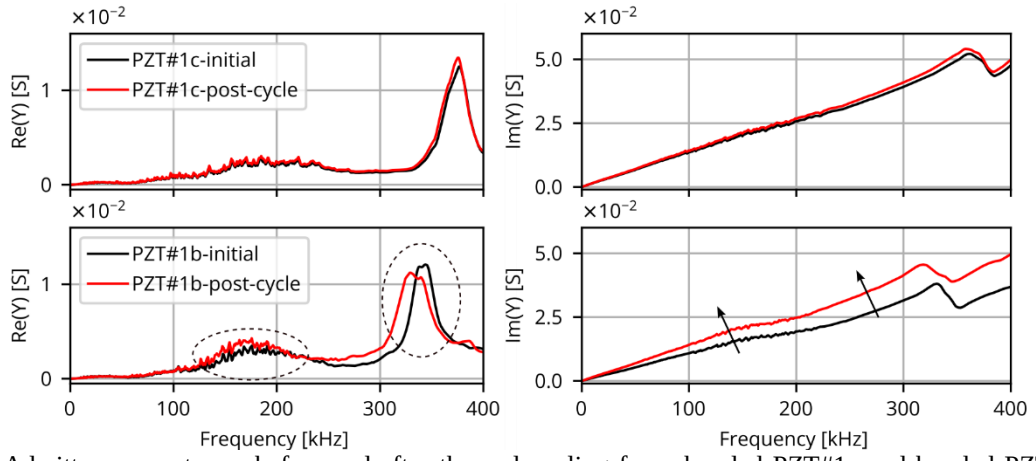

Fig. 4. Admittance spectrums before and after thermal cycling for cobonded PZT#1c and bonded PZT#1b. Dotted circles denote the presence of debonding signatures that can be used for the diagnostic of the PZT transducers.

We can notice on the real part of the admittance spectrum for bonded PZT#1b the clear signature of the debonding circled on Fig. 4., very similar to debonding signature identified in [1], [2]. This signature on the real part of the spectrum is observed on both PZT (#1b and #2b) with detected debondings in LDV. The imaginary part of the spectrum presents an increase in slope that is not linked to the debonding as PZT#2b (without debonding) exhibits the same evolution; it can therefore be assumed that this is linked to an evolution of the

bonding layer properties or the PZT properties. In contrast, the admittance spectrums of the cobonded PZTs show a great stability to the thermal cycling which was expected due to the stability of the composite material in this temperature.

3.2 FBG diagnostic through their reflection spectrum

One measurement that can potentially give some information about the health state of the FBG sensors is the shape of its reflection spectrum. The shape of the spectrum is impacted in the presence of non-uniform strain fields as illustrated in [9] for example. In the presence of partial debonding of the FBG, non-uniform strains will likely be induced in the sensors and therefore lead to a distortion of the reflection spectrum. Thus, concerning the diagnostic of an FBG as an SHM sensor, the monitoring of the FBG spectrum shape could be used to detect the presence of sensor debonding.

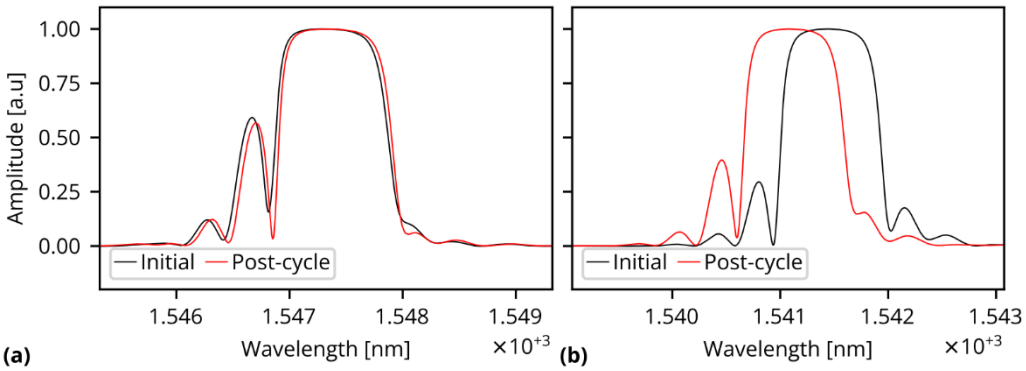

Fig. 5. FBG reflection before and after thermal cycling for the cobonded (a) and the bonded (b) FBG

We can see that for both bonding methods, the reflection spectrum of the FBG show very little distortions and therefore are expected to be relatively unscathed by the thermal cycling. For the bonded FBG we can see a small horizontal shift that is associated to the release of residual stress built up during the adhesive curing.

4. Impact damage detection

4.1 Incremental impact tests

Impact damage is induced in the first composite plate using a drop weight impact test machine. In addition to GW and sensor diagnostic acquisition, a flash thermography of the backside of the impacted area is performed between each impact to control the increase in damage size. Fig. 6 shows the thermography images for the highest values of impact energy. At lower energy, the damage remains barely visible. As it can be seen on the thermography images, the damage is very anisotropic; therefore, the influence on the GW signal is likely to vary a lot depending on the angle at which the GW path crosses the impact location.

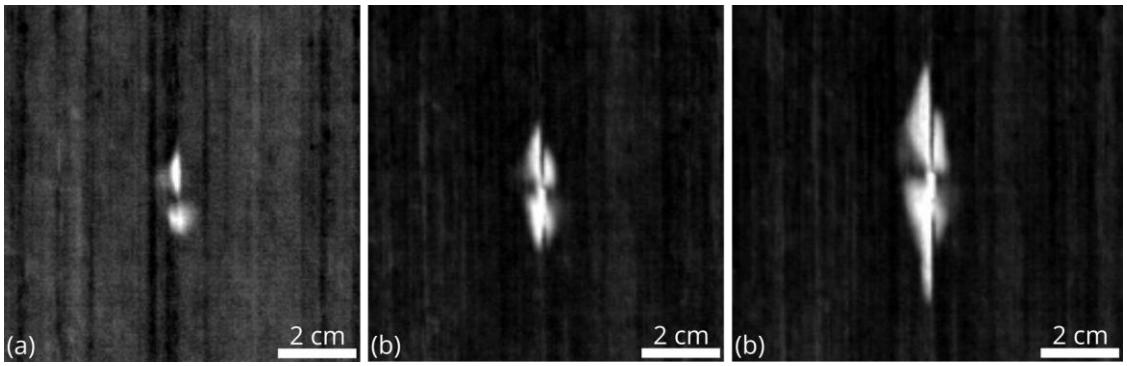

Fig. 6. Flash thermography images of the resulting damage after an impact energy of 7.5 J (a), 10 J (b) and 12.5 J (c). Damage at lower impact energy is barely visible.

4.2 Damage index evaluation

The SDC damage index is computed from the GW signals after each impact on the first plate and after the thermal cycling on the second one. The results are presented Fig. 7 for the cobonded sensors and Fig. 8 for the bonded sensors.

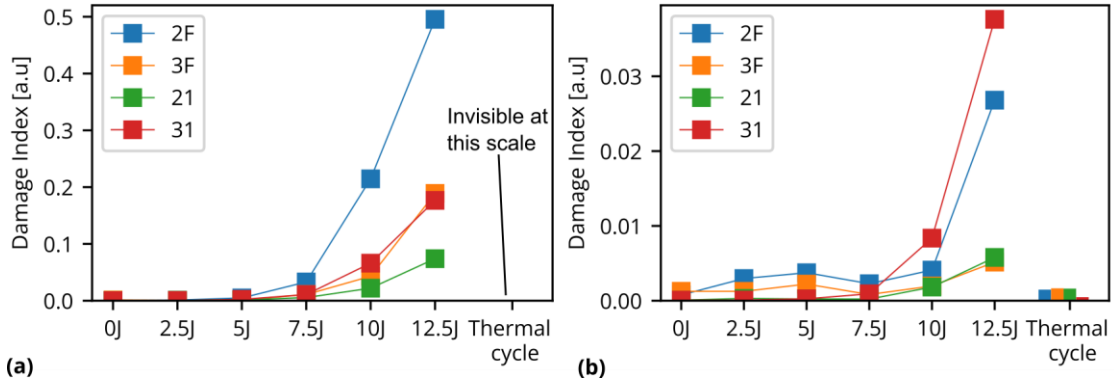

Fig. 7. DI computed for the different signal paths at different impact energy levels and after thermal cycling, at 25 kHz (a) and 200 kHz (b) for the cobonded system.

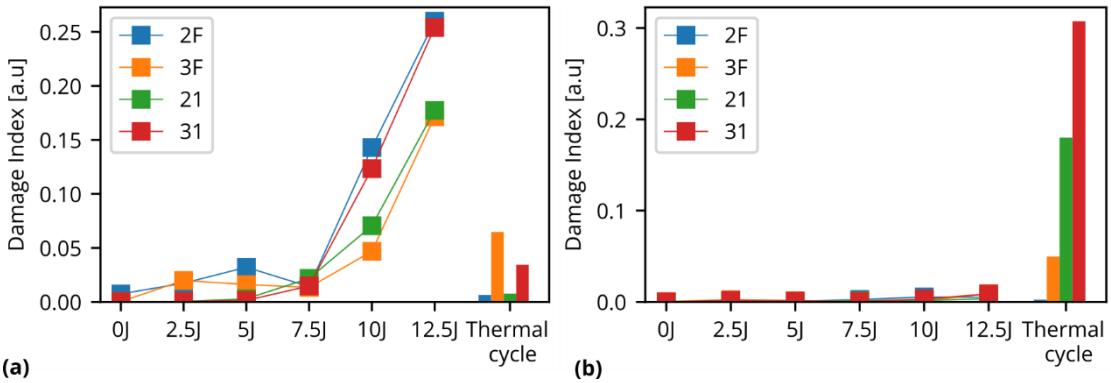

Fig. 8. DI computed for the different signal paths at different impact energy levels and after thermal cycling, at 25 kHz (a) and 200 kHz (b) for the bonded system.

First, it can be noticed that the impact damage has a much higher signature at 25 kHz, ie for the A0 mode, than for the S0 mode at 200 kHz. Nevertheless, both frequencies could be used to detect the damage in that case. A larger sample size would be needed to clearly determine a threshold for damage detection taking into account all the possible uncertainties (material properties, environmental conditions etc.) however, it seems likely that the damage generated by impact energies higher than 10 J will be detected. Additionally, it can be seen

that the thermal cycle has very little impact on the DI, which was expected, as cobonded sensors did not exhibit any evolution on the diagnostic measurements. This is in stark contrast with the results for the bonded sensors visible in Fig. 8. The signature of the debondings caused by the thermal cycling on the DI at 25kHz is, for the "worst" path, of the same order of amplitude than a 10 J impact, which could definitely lead to some false alerts. The effect of the degradation from the thermal cycling is even stronger at 200 kHz with DI values reaching 0.3, which is more than ten times the value of the DI coming from the actual impact damage. Thus, it would be impossible to use the S0 mode at 200 kHz to detect the impact damage with this extent of degradation of the system. We can also note that the path 2F between PZT#2b (with no detected debonding) and the bonded FBG presents very small DI values: this path could still be used for damage detection.

Conclusions

This paper aims at comparing the influence on GW signals used for damage detection of the damage itself and the thermal aging of the GW SHM system. This comparison was made at 25 kHz and 200 kHz through a common DI based on the cross-correlation with the baseline signals. The DI was able to detect incremental impact damages with an impact energy above 10J with around 10 times the sensitivity at 25 kHz than at 200 kHz. This is likely due to less wave-damage interactions for the S0 mode investigated at 200 kHz.

The thermal cycling had little to no impact on the cobonded sensors, which did not show any significant evolution of the DI that could create some false damage detections. FBG and PZT performed very similarly in that case. This is in good agreement with the diagnostic step that did not detect any significant evolution of these sensors. However, for the bonded sensors, some debondings were detected under two PZT, along with potential evolution of the bonding layer or piezoelectric properties. These degradations caused (at 25kHz) a significant increase in the DI, up to values that could correspond to a 10J impact detection and thus lead to false detection if the diagnostic step is not used to invalidate the faulty sensors. At 200 kHz the influence of the PZT debondings is even more significant with a DI value more than 10 times higher than the one of the 12.5J impact. Therefore, this higher frequency seems to be less sensitive to the impact damage while being more impacted by the thermal aging of the sensors and thus the lower frequencies using the A0 mode should be preferred for this configuration. Finally, if we consider the path where the diagnostic step did not detect any debonding of the sensors, the DI is much less impacted by the thermal cycling and should still be able to detect the damage without a false detection.

It is likely that these results strongly depend on the choice of the DI; therefore, other common DI formulations are being tested for this case and will be discussed at the conference.

References

[1] I. Mueller and C.-P. Fritzen, 'Inspection of Piezoceramic Transducers Used for Structural Health Monitoring', *Materials*, vol. 10, no. 1, p. 71, Jan. 2017, doi: 10.3390/ma10010071.

[2] L. Mastromatteo, L. Gaverina, F. Lavelle, J.-M. Roche, and F.-X. Irisarri, 'Thermal Cycling Durability of Bonded PZT Transducers Used for the SHM of Reusable Launch Vehicles', in *European Workshop on Structural Health Monitoring*, vol. 254, P. Rizzo and A. Milazzo, Eds., in Lecture Notes in Civil Engineering, vol. 254. , Cham: Springer International Publishing, 2023, pp. 727–736. doi: 10.1007/978-3-031-07258-1_73.

[3] V. Memmolo, Y. J. Park, M. Lilov, E. Monaco, and F. Ricci, ‘Preliminary acousto-ultrasonic investigation for multi-parameter transducer self-diagnostic system in composites’, *Composite Structures*, vol. 202, pp. 1229–1238, Oct. 2018, doi: 10.1016/j.compstruct.2018.05.125.
[4] M. Philibert, K. Yao, M. Gresil, and C. Soutis, ‘Lamb waves-based technologies for structural health monitoring of composite structures for aircraft applications’, *European Journal of Materials*, vol. 2, no. 1, pp. 436–474, Dec. 2022, doi: 10.1080/26889277.2022.2094839.
[5] V. Giurgiutiu, *Structural Health Monitoring: with Piezoelectric Wafer Active Sensors*. Elsevier, 2007.
[6] R. Soman, J. Wee, and K. Peters, ‘Optical Fiber Sensors for Ultrasonic Structural Health Monitoring: A Review’, *Sensors*, vol. 21, no. 21, p. 7345, Nov. 2021, doi: 10.3390/s21217345.
[7] M. Dziendzikowski, K. Dragan, and A. Katunin, ‘Localizing impact damage of composite structures with modified RAPID algorithm and non-circular PZT arrays’, *Archiv.Civ.Mech.Eng*, vol. 17, no. 1, pp. 178–187, Mar. 2017, doi: 10.1016/j.acme.2016.09.005.
[8] B. Zhang *et al.*, ‘An integrated numerical model for investigating guided waves in impact-damaged composite laminates’, *Composite Structures*, vol. 176, pp. 945–960, Sep. 2017, doi: 10.1016/j.compstruct.2017.06.034.
[9] Y. Bai, J. Zeng, J. Huang, Z. Cheng, Q. Zhao, and D. Liang, ‘Non-uniform strain field reconstruction of FBG using an adaptive Nelder–Mead algorithm’, *Optics Communications*, vol. 484, p. 126689, Apr. 2021, doi: 10.1016/j.optcom.2020.126689.